

1 This manuscript is an *EarthArXiv* preprint and has not yet undergone peer-review. It is  
2 currently submitted to *MDPI - Atmosphere*. Hence, its final accepted version may be different  
3 from the current one. Once the manuscript will be fully published the corresponding DOI  
4 link will be added on the right-hand side of this webpage. Please, feel free to contact the  
5 corresponding author if you have any feedback.

## 8 **Past and projected weather pattern persistence with** 9 **associated multi-hazards in the British Isles**

10 **Paolo De Luca<sup>1\*</sup>, Colin Harpham<sup>2</sup>, Robert L. Wilby<sup>1</sup>, John K. Hillier<sup>1</sup>, Christian L. E. Franzke<sup>3</sup> and**  
11 **Gregor C. Leckebusch<sup>4</sup>**

12 <sup>1</sup>Geography and Environment, Loughborough University, Loughborough, UK

13 <sup>2</sup>Climatic Research Unit (CRU), School of Environmental Sciences, University of East Anglia, Norwich, UK

14 <sup>3</sup>Meteorological Institute and Center for Earth System Research and Sustainability (CEN), University of  
15 Hamburg, Hamburg, Germany

16 <sup>4</sup>School of Geography Earth and Environmental Sciences, University of Birmingham, Birmingham, UK

17  
18 \* Correspondence: [87paolo11@gmail.com](mailto:87paolo11@gmail.com)  
19

20 **Abstract:** Hazards such as heatwaves and floods are often linked to persistent weather patterns.  
21 Atmosphere-Ocean General Circulation Models (AOGCMs) are important tools for evaluating  
22 projected changes in extreme weather. Here, we demonstrate that 2-day weather pattern persistence  
23 is a useful concept for both investigating climate risks from multi-hazard events as well as for  
24 assessing AOGCM realism. This study evaluates the ability of a Coupled Model Intercomparison  
25 Project Phase 5 (CMIP5) multi-model sub-ensemble of 10 AOGCMs at reproducing seasonal weather  
26 pattern persistence and frequencies over the British Isles. Changes in persistence are investigated  
27 under two Representative Concentration Pathways (RCP8.5 and RCP4.5) up to 2100. Broadly, the  
28 ensemble replicates historical weather type persistence observed in reanalyses (1971-2000). Future  
29 persistence and frequency of summer anticyclonic patterns are found to increase, implying  
30 heightened risk of drought and heatwaves. On the other hand, the cyclonic weather type decreases  
31 in autumn suggesting reduced likelihood of flooding and severe gales. During winter, AOGCMs  
32 suggest increased risk of concurrent flood-wind hazards by 2100, however, they also tend to over-  
33 estimate such risks when compared to reanalyses. In summer, the strength of the nocturnal Urban  
34 Heat Island (UHI) of London could intensify, enhancing the likelihood of combined heatwave-poor  
35 air quality events. Further research is needed to explore other multi-hazards in relation to changing  
36 weather pattern persistence and how best to communicate such threats to vulnerable communities.

37 **Keywords:** weather patterns; LWTs; persistence; multi-hazards; urban heat island; CMIP5; RCPs  
38

---

39 **1. Introduction**

40 Persistent weather patterns can translate into hazards such as heatwaves, poor air quality,  
41 drought, wildfires and episodes of flooding [1–4], with significant socio-economic losses [5,6].  
42 Examples of such impactful episodes include the 2003 and 2010 European summer heatwaves that  
43 led to more than 100,000 deaths, reduced gross primary productivity of crops and, in the latter  
44 episode over Russia, about US\$15 billion economic losses [7–10]. Similarly, summer 2013 in eastern  
45 China, was the hottest ever recorded in that region, with persistent and widespread heatwaves and  
46 droughts causing severe socio-economic impacts amounting to 59 billion RMB in losses [11].  
47 Conversely, the extremely wet and stormy 2013/14 winter over the United Kingdom (UK) was  
48 characterised by the passage of numerous low-pressure systems causing extensive pluvial, fluvial,  
49 coastal and groundwater flooding along with severe gales [12–14].

50  
51 Natural hazards pose a significant socio-economic threat, yet their spatio-temporal co-  
52 occurrence (termed herein *multi-hazards*) are not yet fully understood [15,16]. Multi-hazards/risks  
53 research has developed considerably over the last decade [17–21], such that the United Nations  
54 Sendai Framework for Disaster Risk Reduction (UNISDR) [22] has called for multi-hazard  
55 approaches to disaster risk reduction. Examples of multi-hazard studies include interactions between  
56 earthquakes and landslides [23], multi-basin flooding and extra-tropical cyclones [24], river and  
57 coastal flooding [25], and extreme wet and dry hydrological events [26–28]. Considering natural  
58 hazards as physical processes that can interact across both temporal and spatial scales is of interest  
59 to decision makers such as governments, local businesses, emergency management services and (re)-  
60 insurance companies. Until recently, natural hazards were almost always considered as independent  
61 perils. However, since they can compound in various ways (i.e. occur simultaneously, as cascades or  
62 cumulatively) over a sufficiently long time-frame [22], their combined socio-economic impacts can  
63 exceed what was originally planned for, putting societies and economies under stress [15].

64  
65 Previous studies have investigated linkages between weather patterns (or large-scale  
66 atmospheric circulation) and local extreme events, such as heavy rainfall, storms, floods and  
67 heatwaves [24,29–36]. The conventional approach to flood analysis at the *single* catchment scale is  
68 being extended to frameworks with inter-related hazards, driven by global climate modes, covering  
69 *multiple* catchments [30]. Others show that the bias in simulating regional extreme precipitation days  
70 by an Atmosphere-Ocean General Circulation Model (AOGCM) is reduced by applying atmospheric  
71 circulation indices [32]. Moreover, weather patterns extracted from AOGCMs have also been used to  
72 downscale local climate variables, such as temperature, precipitation, radiation and humidity at local  
73 scales [34,37,38]. However, AOGCMs vary in their ability to simulate the frequency, seasonality and  
74 persistence of weather patterns at regional scales [33,34]. Some studies have linked heavy  
75 precipitation events to atmospheric circulation states, such as the 850hPa geopotential height field or  
76 integrated vapour transport (IVT) [31], and found connections between objectively-defined weather  
77 patterns, or Lamb Weather Types (LWTs) [39–41], and multi-basin flooding driven by extra-tropical  
78 cyclones (ETCs) [24]. Others have used LWTs to quantify changes in the strength of the *nocturnal*  
79 *Urban Heat Island (UHI)* – a phenomenon that may be associated with combined heatwave and air  
80 pollution events within cities [29]. The LWTs classification scheme, although initially developed for

81 the UK [24,36,50–55,42–49], was also recently applied in other mid-latitude regions, for example  
82 Sweden [e.g. 55,56], the Iberian Peninsula [e.g. 57,58] and Spain [e.g. 59,60].

83

84 Previous evaluations for Europe and the British Isles (BI) show that Coupled Model  
85 Intercomparison Project Phase 5 (CMIP5) AOGCMs generally reproduce LWTs, calculated using  
86 daily sea-level pressure (SLP) fields, but there are recognized biases [45,46]. For example, CMIP5  
87 AOGCMs are not yet able to simulate correctly the number of anticyclonic (A-type) patterns and  
88 hence blocking episodes, with the former being underestimated in northern Europe and the BI, but  
89 overestimated in southern Europe [45,46,62]. Other biases are found for cyclonic (C-type) and  
90 westerly (W-type) occurrences, with both being overestimated across Europe [46]. These studies also  
91 examined future changes in frequency of LWTs and blocking episodes by comparing historical  
92 conditions with RCP8.5, to determine how such changes might affect European temperatures. The A-  
93 type is projected to increase significantly over the BI during all seasons except for winter (DJF), the  
94 C-type to decrease in all seasons, and the W-type to increase except in summer (JJA) by the end of  
95 the century [46]. Overall, blocking episodes are projected to decrease for the BI in DJF and JJA by  
96 2061-2090 (RCP8.5) [62].

97

98 We extend these analyses by assessing the ability of a CMIP5 [63] multi-model sub-ensemble  
99 (MME) of 10 AOGCMs at reproducing historical seasonal persistence of daily LWTs over the BI [39–  
100 41,43]. We define 2-day persistence as the probability that a given LWT will occur on any two  
101 successive days. Climate model simulations of historic LWTs are compared with those derived from  
102 20CR [64], NCEP [65] reanalyses, and Lamb’s catalogue of subjectively defined weather types [39,66].  
103 We investigate how persistence and seasonal frequencies are projected to change within the full 21<sup>st</sup>  
104 century under RCP8.5 and RCP4.5, with persistence assessed for both the MME mean (MMEM) and  
105 individual AOGCMs. We also quantify and discuss the implications of future multi-hazards, here  
106 identified as nearly concurrent multi-basin flooding and ETCs impacting Great Britain (GB) in winter  
107 [24] or combined summer heatwave and poor air quality events over London [29]. Thus, two multi-  
108 hazard metrics are applied, along with their evaluation under RCP8.5 and RCP4.5 projections up to  
109 2100. These are the likelihood of (1) multi-basin flooding (*F-Score*) and (2) changing intensity of the  
110 nocturnal UHI.

111

112

## 113 **2. Methods and Data**

### 114 *2.1 Lamb Weather Types (LWTs)*

115 Daily atmospheric sea-level pressure (SLP) patterns are categorized using the system of LWTs  
116 [39] via an objective classification scheme centred over the BI (Figure 1) [40,41]. Choice of the LWTs  
117 objective scheme is justified by the fact that this methodology and weather typing classification was  
118 originally developed for the BI. LWTs of similar airflow properties are derived from a 5° by 10°  
119 latitude-longitude grid array (Figure 1) and computed from daily (12 UTC) SLP values at each grid  
120 point. The airflow characteristics are expressed by the following set of equations, where the integers  
121 in bold correspond to the grid point reference numbers in Figure 1:

122

123 
$$W = \frac{1}{2}(\mathbf{12} + \mathbf{13}) - \frac{1}{2}(\mathbf{4} + \mathbf{5}) \quad (\text{westerly flow}) \quad (1)$$

124

125 
$$S = 1.74 \left[ \frac{1}{4}(\mathbf{5} + 2.0 \times \mathbf{9} + \mathbf{13}) - \frac{1}{4}(\mathbf{4} + 2.0 \times \mathbf{8} + \mathbf{12}) \right] (\text{southerly flow}) \quad (2)$$

126

127 
$$F = (S^2 + W^2)^{1/2} \quad (\text{resultant flow}) \quad (3)$$

128

129 
$$ZW = 1.07 \left[ \frac{1}{2}(\mathbf{15} + \mathbf{16}) - \frac{1}{2}(\mathbf{8} + \mathbf{9}) \right] - 0.95 \left[ \frac{1}{2}(\mathbf{8} + \mathbf{9}) - \frac{1}{2}(\mathbf{1} + \mathbf{2}) \right]$$

130 
$$\quad (\text{westerly shear vorticity}) \quad (4)$$

131

132 
$$ZS = 1.52 \left[ \frac{1}{4}(\mathbf{6} + 2.0 \times \mathbf{10} + \mathbf{14}) - \frac{1}{4}(\mathbf{5} + 2.0 \times \mathbf{9} + \mathbf{13}) - \frac{1}{4}(\mathbf{4} + 2.0 \times \mathbf{8} + \mathbf{12}) \right]$$

133 
$$\quad + \frac{1}{4}(\mathbf{3} + 2.0 \times \mathbf{7} + \mathbf{11}) \quad (\text{southerly shear vorticity}) \quad (5)$$

134

135 
$$Z = ZW + ZS \quad (\text{total shear vorticity}) \quad (6)$$

136

137 Flow units are derived from the geostrophic approximation (each equivalent to 1.2 knots) and  
138 they are, along with the geostrophic vorticity units, expressed as hPa per 10° latitude at 55°N (100  
139 units are equivalent to  $0.55 \times 10^{-4} = 0.46$  times the Coriolis parameter at 55°N). Three coefficients are  
140 used within equations (2, 4 and 5) to account for variations in relative grid spacing at different  
141 latitudes with latitude ( $\psi$ ) here set as 55° [41]:  $S$  is multiplied by 1.74, derived from  $1/\cos(\psi)$ ;  $ZW$ , 1.07  
142 and 0.95 from  $\sin(\psi)/\sin(\psi-5^\circ)$  and  $\sin(\psi)/\sin(\psi+5^\circ)$ ;  $ZS$ , 1.52 from  $1/2(\cos(\psi)^2)$ .

143

144 The last step for defining LWTs is to apply five rules [39–41]:

145

146 1. the flow direction is given by  $\tan^{-1}(W/S)$  and is calculated on an eight-point compass with 45°  
147 per sector. If  $W$  is positive, add 180°. Thus, the  $W$ -type occurs between 247.5° and 292.5°;

148

149 2. Lamb pure directional weather types (e.g. N, S, or E-types) correspond to an essentially  
150 straight flow, when  $|Z|$  is less than  $F$ ;

151

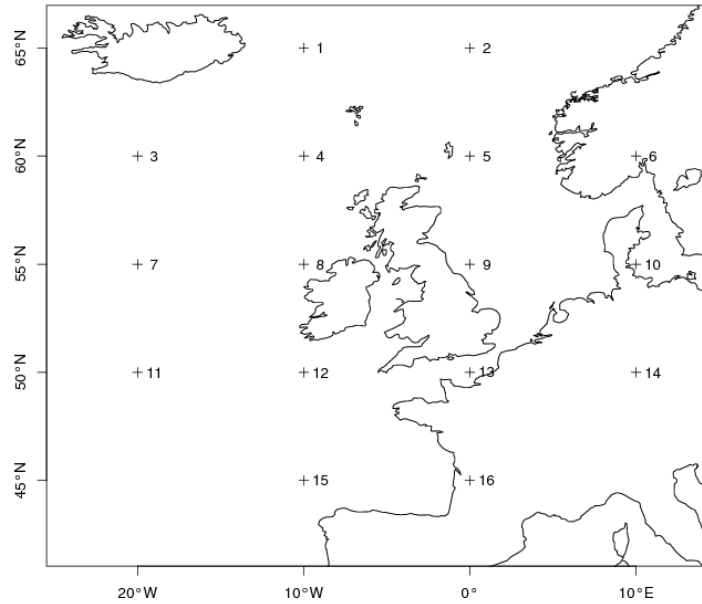
152 3. Lamb's pure cyclonic (C) and anticyclonic (A) types are identified when  $|Z|$  is greater than  
153  $2F$ , respectively with  $Z > 0$  and  $Z < 0$ ;

154

155 4. Lamb's hybrid types (e.g. AE and CSW) are characterised by a flow partially  
156 anticyclonic/cyclonic, with  $|Z|$  lying between  $F$  and  $2F$ ;

157

158 5. the unclassified (U) type is obtained when  $F$  and  $|Z|$  are less than 6, with the choice of 6  
159 depending on grid spacing.



160  
 161  
 162  
 163  
 164  
 165  
 166  
 167  
 168  
 169  
 170  
 171  
 172  
 173  
 174  
 175  
 176  
 177  
 178  
 179  
 180  
 181  
 182  
 183  
 184  
 185  
 186  
 187  
 188

**Figure 1. Grid points used to calculate Jenkinson flow and vorticity terms for the British Isles (BI).**  
 Numbers refer to those points used in Equations 1 to 5.

The objective classification scheme yields 27 LWTs comprised of two synoptic types (A and C), five purely directional types (W, NW, E, N, and S), 19 hybrid combinations of synoptic and directional types (e.g. CNW, CSE and AE), and 1 unclassified (U) type [40,41]. For persistence and frequency analyses, we focus on the 7 synoptic and directional LWTs plus the U-type; counts of hybrid types were spread across the main types as per Lamb’s original definition [39,67] and common practice within earlier studies [40,43,68,69]. We assess LWT persistence and frequency for summer (June-July-August, JJA), autumn (September-October-November, SON), winter (December-January-February, DJF) and spring (March-April-May, MAM). On the other hand, when calculating indices of future multi-hazards, the hybrid LWTs were not incorporated into the 7 main types as the F-Score and nocturnal UHI indices require these weather patterns to be considered independently.

## 2.2 Data

Weather patterns were derived from the SLP produced by each AOGCM in our CMIP5 MME listed in Table 1 [63]. We defined the historical period as the 1980s (1971-2000) whereas the future was divided into three 30-year periods: the 2020s (2011-2040), 2050s (2041-2070) and 2080s (2071-2100). The CMIP5 AOGCMs and MMEM outputs for the historical period was compared with LWTs derived from 20CR [64], NCEP [65] reanalyses and Lamb’s subjective catalogue, which ends in 1997 [39,66]. The MMEM was built by first computing the LWTs and relative seasonal persistence and frequencies per each AOGCM then averaging these values within each time-period. The choice of the models included in our MME (Table 1) reflects a range of research institutes running similar boundary forcing experiments.

**Table 1. CMIP5 multi-model sub-ensemble (MME) used in the analyses.**

Model name	Research institute	Lat-Lon resolution	Ensemble member
HadGEM2-ES	Met Office, United Kingdom	1.25° × 1.875°	r1i1p1
MPI-ESM-LR	Max Planck Institute for Meteorology, Germany	1.9° × 1.9°	r1i1p1
MRI-CGCM3	Meteorological Research Institute, Japan	1.1° × 1.1°	r1i1p1
CNRM-CM5	National Centre for Meteorological Research, France	1.4° × 1.4°	r1i1p1
CanESM2	Canadian Center for Climate Modeling and Analysis, Canada	2.8° × 2.8°	r1i1p1
MIROC5	Model for Interdisciplinary Research on Climate, Japan	1.4° × 1.4°	r1i1p1
CSIRO-Mk3.6.0	Commonwealth Scientific and Industrial Research Organisation, Australia	1.9° × 1.9°	r10i1p1
IPSL-CM5A-LR	Institute Pierre-Simon Laplace, France	1.9° × 3.75°	r1i1p1
CCSM4	National Center for Atmospheric Research, USA	0.94° × 1.25°	r6i1p1
GFDL-CM3	Geophysical Fluid Dynamics Laboratory, USA	2° × 2.5°	r1i1p1

190 The columns in Table 1 show the: (1) CMIP5 model name; (2) research institute where the model was  
 191 developed; (3) resolution for latitude by longitude in degrees; and (4) ensemble member analysed.  
 192 For all models the historical and RCP8.5 (and RCP4.5) sea-level pressure (SLP) outputs are used to  
 193 calculate daily LWTs for the BI.

194

195

### 196 2.3 Persistence and trend analyses

197 Weather pattern persistence is defined here as the conditional probability ( $p_{jj}$ ) that a given LWT<sub>*j*</sub>  
 198 on day(*t*) is followed by the same LWT<sub>*j*</sub> on day(*t*+1) [70,71]. This diagnostic was extracted for the 7  
 199 main LWTs and the U-type using the diagonal cells of Markov-chain transition matrices. This enabled  
 200 estimation of historical (1980s) and future (2020s, 2050s and 2080s) seasonal persistence for the  
 201 MMEM as well as for individual AOGCMs for impactful weather types and seasons, the 20CR, NCEP  
 202 reanalyses and Lamb's subjective catalogue.

203

204 Uncertainty in  $p_{jj}$  for the 1980s was calculated by boot-strapping ( $n=1,000$ ) 30-year seasonal  
 205 simulations using the *markovchain* package within the R framework [72]. This algorithm stochastically  
 206 generates  $n$  series of daily LWTs from the original conditional distributions of the weather patterns  
 207 in each AOGCM, then recomputes  $p_{jj}$  from each series. The resulting  $p^{BOOTSTRAP}_{jj}$  is the mean of all  $p_{jj}$   
 208 across the 1000 series, for each AOGCM. The 95% confidence intervals of  $p^{BOOTSTRAP}_{jj}$  are obtained from  
 209 the cumulative distribution of the 1000 values of  $p_{jj}$  for each AOGCM.

210

211 Statistical significance of changes in persistence for the AOGCM sub-ensemble between the 1980s  
212 and future periods (Tables S1-S2) was assessed using a Mann-Whitney-Wilcoxon two-tailed test [73]  
213 applied to the 10 estimates of  $p^{BOOTSTRAP_{ij}}$  for each time period. Changes in  $p_{ij}$  between the 1980s and  
214 future periods for individual AOGCMs were regarded as statistically significant if future persistence  
215 of a given LWT and AOGCM fell outside the 95% confidence intervals of the  $p^{BOOTSTRAP_{ij}}$  range of that  
216 AOGCM for the 1980s (Figures 3 and S2).

217

218 To detect both linear and non-linear annual changes in the total seasonal counts of LWTs MMEM  
219 frequencies under RCP8.5 and RCP4.5 scenarios, a trend analysis was performed for the 2006-2100  
220 time period. For illustrative purposes, we only show trends for anticyclonic (A, summer JJA), cyclonic  
221 (C, autumn SON) and westerly (W, winter DJF) types as indicators of impactful weather across the  
222 BI (Figures 4 and S3). Results are also presented for the southerly (S, spring MAM) types as this LWT  
223 shows most significant changes in seasonal persistence according to the non-parametric Mann-  
224 Whitney-Wilcoxon two-tailed test between the 1980s and each of the three future periods (i.e. 2020s,  
225 2050s and 2080s). A modified Mann-Kendall test, which takes into account possible autocorrelation  
226 within the time series, was applied to both RCP8.5 and RCP4.5 seasonal MMEM LWTs frequencies  
227 [74]. The significance of trends, along with their relative Sen's slopes, are shown in Table S3 [75].

228

#### 229 2.4 Indices of winter flood-wind hazards and summer UHI intensity

230 As a measure of concurrent flood-wind hazards we calculated an extended version of the F-  
231 Index [24,76], here defined as the F-Score, for each AOGCM, MMEM, NCEP, 20CR and Lamb's  
232 subjective catalogue, covering the 1980s, 2020s, 2050s and 2080s, for selected LWTs known to drive  
233 these multi-hazard events [24] during winter under both RCP8.5 (Figure 5) and RCP4.5 (Figure S4).  
234 The F-Index is the ratio of observed to expected frequency of floods for a given LWT, where values  
235 greater than 1 show higher than expected likelihood. Ten LWTs are known to be associated with  
236 historic, multi-basin floods [24], of which eight (C, CS, CSW, CNW, S, SW, W, and NW-types) increase  
237 their likelihood and two (N and A-types) reduce likelihood. All other LWTs are weighted zero. The  
238 F-Score is then calculated by multiplying the winter DJF frequencies ( $freq\_djf_j$ ) of these LWTs by  
239 their  $F\_Index_j$  (as per Event Set E in [24]) and by summing these values:

240

$$241 \quad F\_Score_i = \sum_{j=1}^{10} freq\_djf_{i,j} \times F\_Index_{i,j} \quad (7)$$

242

243 where  $i$  represents the single AOGCM, NCEP, 20CR and Lamb's subjective datasets within the  
244 relative time periods of 1980s, 2020s, 2050s, 2080s and  $j$  is the given LWT considered from the 10  
245 types mentioned above. The higher the F-Score, the greater the likelihood of concurrent multi-basin  
246 flood and wind hazards within winter, over the specified time horizon and RCP scenario.

247

248 As a proxy for combined heatwave and poor air quality hazards occurring during summer, we  
249 use observed, simulated and projected nocturnal UHI temperatures in tenths of degree Celsius for  
250 London (UK) [29], using the same datasets, time periods and RCPs as per the F-Score (Figures 6 and

251 S5). The UHI phenomenon is caused by absorption and trapping of heat as well as by changed  
 252 airflows and sensible heat fluxes within the built environment. The simplest form of UHI metric (used  
 253 by [29]) is based on the daily temperature difference between an urban and rural reference site  
 254 (during daylight or night hours). These values may then be stratified by LWT to show the extent to  
 255 which some weather patterns favour extreme UHI episodes. The UHI metric was derived as follows  
 256 by: i) multiplying LWT summer JJA frequencies ( $freq\_jja_h$ ) by their respective average UHI  
 257 intensities taken from [29] ( $UHI\_w_h$ ); ii) summing these values; and iii) dividing the total from step ii)  
 258 by the number of days in the period analysed ( $days_h$ ) to give the mean daily UHI intensity:  
 259

$$260 \quad UHI_i = \sum_{h=1}^{27} \frac{freq\_jja_{i,h} \times UHI\_w_{i,h}}{days_{i,h}} \quad (8)$$

261  
 262 where  $i$  is the same notation as per the F-Score and  $h$  refers to the 27 LWTs.  
 263

264 To assess the statistical significance of changes between the AOGCMs 1980s and future 2020s,  
 265 2050s and 2080s periods, for both the F-Score and nocturnal UHI temperatures, we applied a similar  
 266 approach as per persistence. Here,  $n=1,000$  boot-strapped samples of daily LWT series (based on  
 267 conditional distributions for all seasons combined) were generated for each AOGCM run in the 1980s.  
 268 Next, the F-Score or UHI were calculated for every series and AOGCM, then averaged and confidence  
 269 limits established as before. This procedure shows the extent to which estimates for the future indices  
 270 fall within the 95% confidence range of the boot-strapped estimate for each AOGCM in the 1980s.  
 271

272 Sample sizes varied depending on the index and AOGCM. For the F-Score, we considered the  
 273 period 1971-2001 to capture January and February of winter 2000/01. Here, models with leap years  
 274 have a total of 11,323 days, models without leap years 11,315 days and the HadGEM2-ES model (with  
 275 360 days per year) has 11,160 days. For the UHI, the calendar years 1971-2000 were used as we are  
 276 interested in summer temperatures, with leap year AOGCMs having 10,958 days, non-leap years  
 277 models 10,950 days and the HadGEM2-ES 10,800 days.  
 278  
 279

### 280 **3 Results**

#### 281 *3.1 Persistence of weather patterns (MME)*

282 The A, C and W patterns are the most frequent weather types affecting the BI. Overall, the MME  
 283 replicates weather type persistence during the four climatological seasons when compared with 20CR  
 284 [64] and NCEP [65] reanalyses for the historical period (1980s) (Figure 2). There is less agreement  
 285 between Lamb's subjectively classified daily weather catalogue and both the MME and reanalyses.  
 286 A-type persistence is more variable within the MME and on average underestimated in winter,  
 287 consistent with previous studies [45,46]. There is closer agreement for the A-type in other seasons.  
 288

289 W-type persistence agrees with the reanalyses but is always less than in Lamb's catalogue. C-  
 290 type persistence is overestimated by the MME in all seasons when compared to reanalyses as



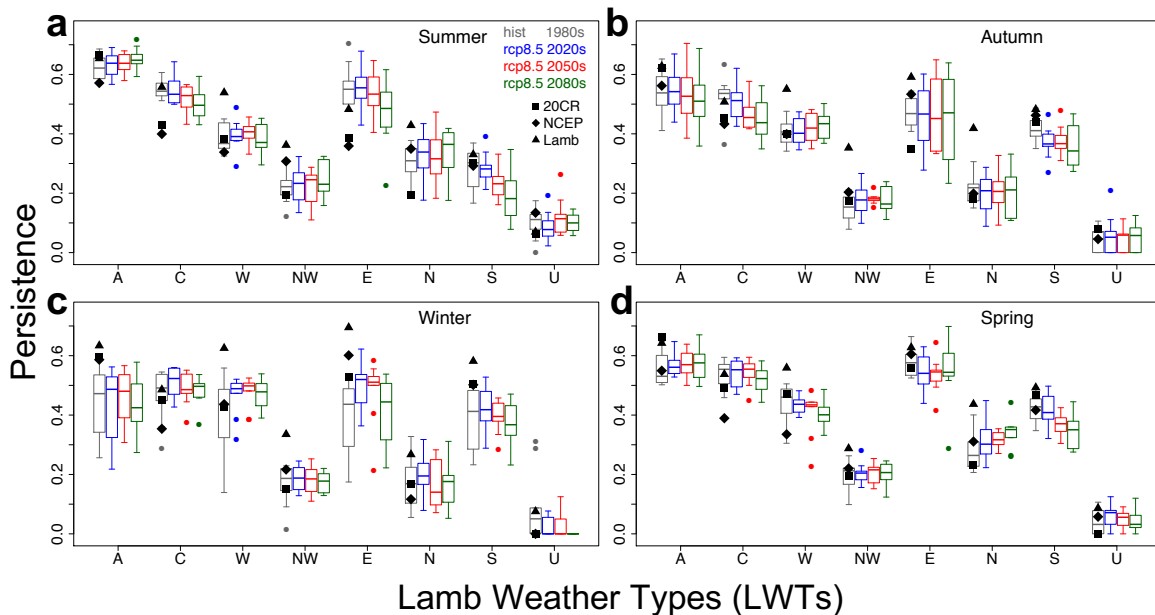
291 reported before [46] for Europe more generally. Such biases in the C-type could be interpreted as  
 292 exaggerating the likelihood of flooding in the MME compared with reanalyses [76].

293

294 Figure 2 shows that the distributions of persistence are asymmetrical (or skewed) around the  
 295 MME means for many of the weather types and time periods. This characteristic suggests potentially  
 296 large biases in the estimation of extreme events, if studies rely on a single AOGCM. Changes in  
 297 weather type persistence between the ensembles of historical and future periods within RCP8.5  
 298 (Figure 2) are weakly significant ( $p$ -value $<0.1$ , Mann-Whitney-Wilcoxon two-tailed test) for the C-  
 299 type in summer and autumn by 2080s; W-type in winter by 2050s; E-type in summer by 2080s and  
 300 winter for the 2020s and 2050s; N-type in spring by 2050s and 2080s; and S-type in summer by 2080s,  
 301 autumn in all periods and spring by 2050s and 2080s (Table S1).

302

303



304

305 **Figure 2. Persistence of the seven main LWTs plus unclassified (U) type under RCP8.5.** Persistence  
 306 is calculated for (a) summer, (b) autumn, (c) winter and (d) spring, for the historical 1980s (1971-2000)  
 307 and under RCP8.5 by the 2020s (2011-2040), 2050s (2041-2070) and 2080s (2071-2100). Boxplots show  
 308 distributions of persistence in each LWT, for the 10-member AOGCM ensemble, compared with  
 309 20CR, NCEP and the Lamb's catalogue. Segments show the minimum, 1<sup>st</sup> quartile, median, 3<sup>rd</sup>  
 310 quartile and maximum. Outliers are shown by dots.

311

312

313 Results for RCP4.5 show similar changes in persistence compared to RCP8.5, although they are  
 314 less substantial (Figure S1). In particular, the C-type is found to change significantly ( $p<0.1$ ) only in  
 315 summer by the 2080s; the E-type in winter by the 2080s; the N-type only in spring by the 2080s; and  
 316 the S-type in summer by the 2050s and spring also by the 2020s (Table S2).

317

### 318 3.2 Persistence of weather patterns (by model)

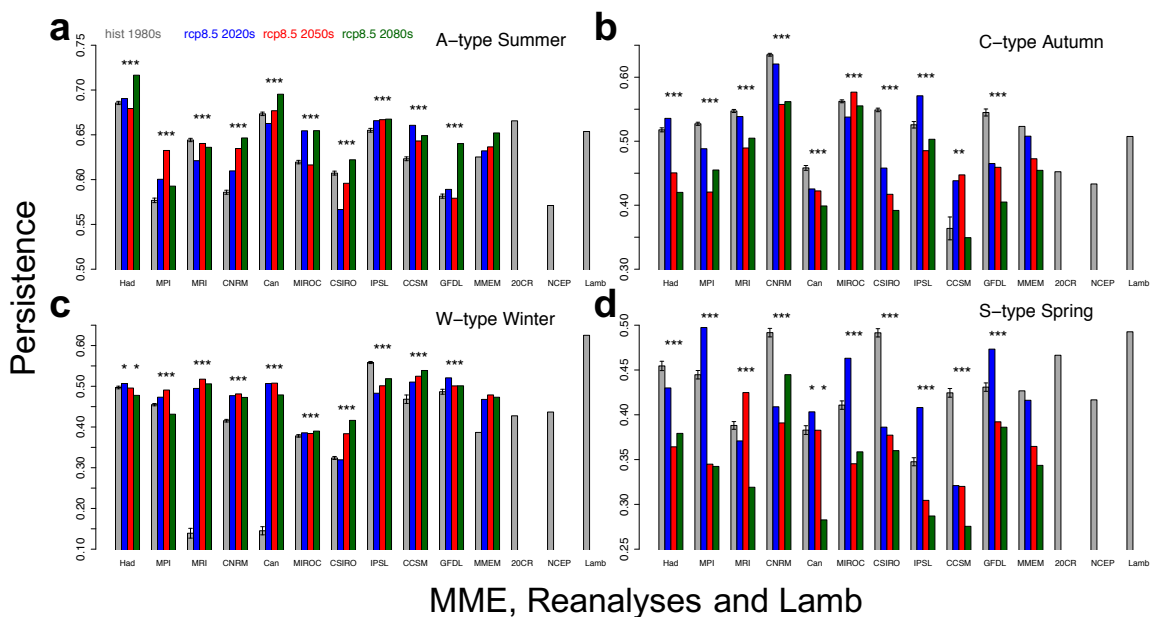
319 Figure 3 shows persistence for the same future periods but for each AOGCM in the MME  
 320 compared with the reanalyses and Lamb's catalogue, for impactful weather types and seasons.  
 321 Significance of changes was assessed against the boot-strapped confidence limits for the 1980s. Most  
 322 model projections under RCP8.5 fall outside the 95% confidence intervals of historical persistence. A-  
 323 type MMEM persistence increases during summer (Figures 2a and 3a); C-type persistence decreases  
 324 in all seasons, most markedly in summer and autumn (Figures 2 and 3b); W-type persistence does  
 325 not change in winter but increases in autumn and decreases in spring (Figures 2b-d and 3c).

326

327 Amongst the other weather types, we note only a decrease in C- and E-types during summer, an  
 328 increase in N-type in spring, and S-type persistence decreases in all seasons (Figures 2 and 3d). The  
 329 AOGCMs showing the largest change in A-type persistence during summer are CNRM-CM5, GFDL-  
 330 CM3 and MIROC5, with a significant increase of 0.06, 0.06 and 0.04 respectively between 1980s and  
 331 2080s. For the C-type in autumn, CSIRO-Mk3.6.0, GFDL-CM3 and HadGEM2-ES show a significant  
 332 decrease in persistence, between 1980s and 2080s, of 0.16, 0.14 and 0.10 respectively. During winter,  
 333 for the W-type, the AOGCMs showing the largest change, between the same 1980s and 2080s periods,  
 334 are MRI-CGCM3, CanESM2 and CSIRO-Mk3.6.0 with a significant increase in persistence of 0.37, 0.33  
 335 and 0.09 respectively.

336

337



338

339 **Figure 3. Persistence of selected LWTs and seasons for individual AOGCMs under RCP8.5.** (a) A-  
 340 type (summer), (b) C-type (autumn), (c) W-type (winter) and (d) S-type (spring) in the 1980s  
 341 compared with the 2020s, 2050s and 2080s under RCP8.5. Persistence is shown for individual  
 342 AOGCMs alongside the MMEM, 20CR, NCEP and Lamb's catalogue. Asterisks (\*) show model runs  
 343 with persistence outside the 95% confidence intervals of the boot-strapped ( $n=1,000$ ) estimates for the  
 344 1980s, shown here as black T-bars.

345

346

347 Analysis of RCP4.5 output shows similar, though less marked, results when compared to RCP8.5  
348 (Figure S2). Under the lower emission scenario, we find that most AOGCMs project persistence that  
349 falls outside the 95% confidence intervals of the 1980s. A-type MMEM persistence in summer could  
350 increase slightly, in particular during the 2080s (Figures S1a-S2a), C-type in autumn may decrease  
351 (Figures S1b-S2b), W-type during winter is projected to remain stable across the three future periods  
352 (Figures S1c-S2c) and S-type persistence in spring decreases by 2100 (Figures S1d-S2d). The C-type  
353 in summer and A-type in autumn exhibit decreased persistence, whereas the E-type shows a marked  
354 increase in persistence during winter; findings that differ from RCP8.5 (Figure S1).

355

### 356 *3.3 Frequency of weather patterns (MMEM)*

357 Projected frequency trends for selected weather types and seasons under RCP8.5 (2006-2100) are  
358 shown in Figure 4. Summer A- and winter W-type frequencies could rise significantly ( $p < 0.01$ , Table  
359 S3) by 0.8 and 0.2 days per decade respectively over the period 2006-2100. Conversely, C- and S-type  
360 frequencies decrease significantly ( $p < 0.01$ , Table S3) in autumn and spring respectively. No  
361 significant trends are found for C-type frequency during winter. Sen's slopes for the MMEM with  
362 their statistical significance are given in Table S3 for each weather type, season and RCP. We also  
363 computed the Sen's slopes for A-type in each AOGCM during summer (RCP8.5, not shown here) to  
364 check whether the increase in A-type was solely due to a few models showing a large increase in this  
365 weather type. We found that all models within the MME show a positive increase in A-type  
366 frequency, with 7 out of 10 AOGCMs showing significance at the 90% level, with no outliers skewing  
367 the MMEM. Among other seasons (not shown), a significant decrease in annual frequencies is  
368 observed for the C-type during summer ( $p < 0.01$ ) and spring ( $p < 0.05$ ), along with a significant ( $p < 0.01$ )  
369 increase in A-type during spring, which all reflect the changes in persistence (Figure 2a and 2d).

370

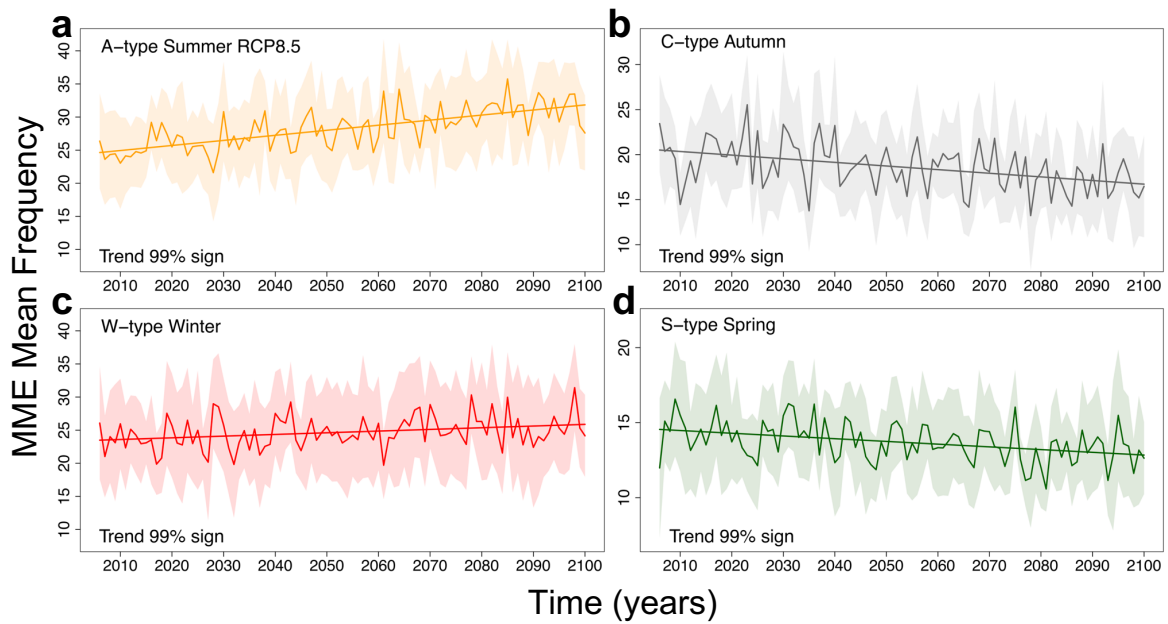
371

372

373

374

375



376

377 **Figure 4. Projected annual frequencies for selected LWTs and seasons under RCP8.5.** Frequencies  
 378 are shown as MMEM for (a) summer anticyclonic A, (b) autumn cyclonic C, (c) winter westerly W  
 379 and (d) spring southerly S LWTs under RCP8.5 (2006-2100). Trends are statistically significant at the  
 380 1% level ( $p$ -value $<0.01$ , modified Mann-Kendall test). Shaded areas represent the 95% confidence  
 381 intervals of the MMEM. The trend lines refer to the Sen's slopes calculated with the modified Mann-  
 382 Kendall test.

383

384

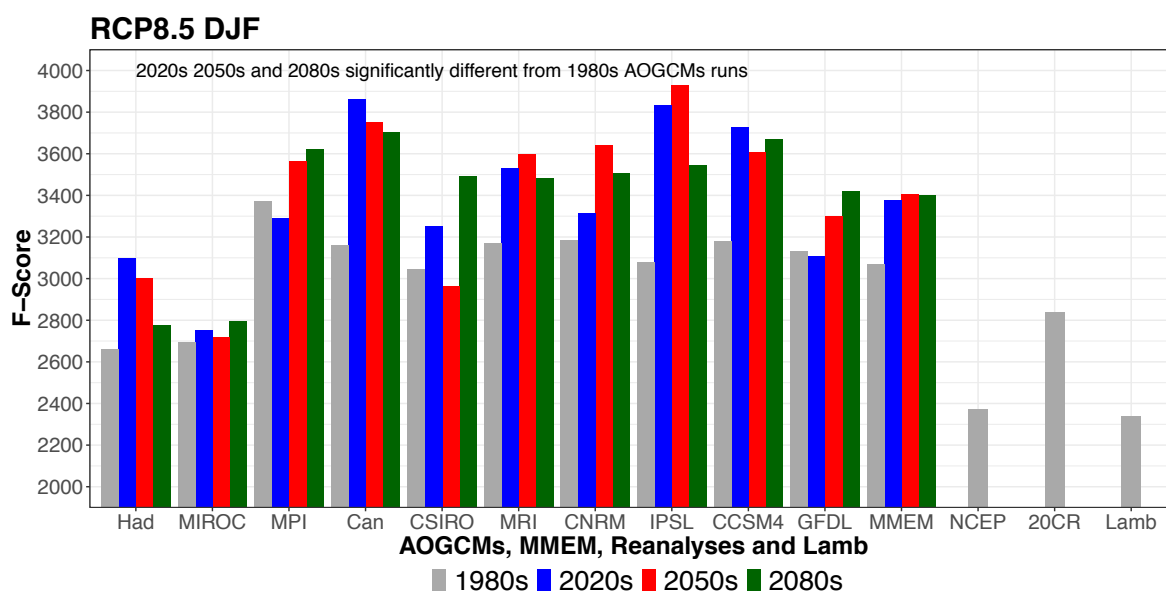
385 Projections of MMEM frequencies for the same LWTs and seasons but under RCP4.5 are shown  
 386 in Figure S3 and Table S3. Results for RCP4.5 reflect the scenarios of RCP8.5 although the Sen's slopes  
 387 are less extreme and statistically significant. The A-type frequency is projected to increase  
 388 significantly ( $p<0.01$ , Figure S3a and Table S3) during summer, C-type in autumn is set to decrease  
 389 ( $p<0.05$ , Figure S3b), W-type frequency in winter shows no significant trend (Figure S3c), and the S-  
 390 type during spring decreases significantly ( $p<0.05$ , Figure S3d). As per RCP8.5, we also observe (not  
 391 shown) a significant decrease in C-type frequencies during summer ( $p<0.01$ ) and spring ( $p<0.05$ ) and  
 392 an increase in the A-type during spring ( $p<0.05$ ), matching the relative changes in persistence (Figure  
 393 S1a and S1d).

394

### 395 3.4 Application to future multi-hazards

396 In Figure 5 we extend an earlier analysis [24] based on impactful LWTs found to generate  
 397 concurrent flood-wind hazards in GB. Thus, the F-Score for each single AOGCM, MMEM, NCEP,  
 398 20CR and Lamb's subjective datasets and 1980s, 2020s, 2050s and 2080s time periods are shown for  
 399 winter DJF weather patterns under RCP8.5. The F-Score is a measure of the severity of future  
 400 concurrent flood-wind hazards, such that higher values represent more severe impacts compared to  
 401 lower ones. Here, we show that the baseline risk from multiple flood-wind hazards is overestimated  
 402 by all but two of the AOGCMs (HadGEM2-ES and MIROC5) when compared to NCEP, 20CR  
 403 reanalyses and Lamb's subjective catalogue for the 1980s. Assuming the same bias holds in the future,

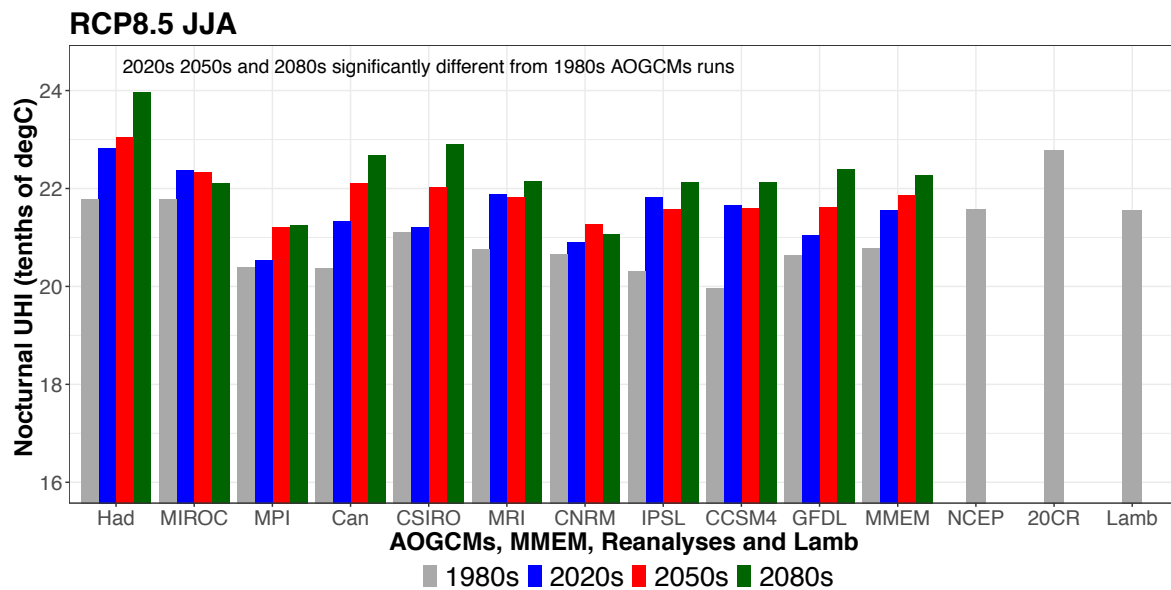
404 the AOGCMs evaluated here likely overestimate *absolute* future risk from concurrent flood-wind  
 405 hazards by 2100. Moreover, in a similar way as per Figure 3, there exists a large variability between  
 406 the AOGCMs, so F-Score results are mixed with some AOGCMs suggesting increased/decreased risk  
 407 of flood-wind hazards by the end of the 21<sup>st</sup> century. Lastly, by looking at the MMEM we conclude  
 408 that, although overestimated by AOGCMs, future risk from concurrent flood-wind hazards could  
 409 increase by 2100 compared with the 1980s. Among the AOGCMs, those showing the largest F-Score  
 410 increase between the 1980s and 2080s are CanESM2, CCSM4 and IPSL-CM5A-LR. Results for RCP4.5  
 411 are shown in Figure S4 and they agree with what was found for RCP8.5, with large variability  
 412 amongst AOGCMs and MMEM F-Score even slightly higher than RCP8.5.  
 413  
 414



415  
 416 **Figure 5. F-Score for LWTs associated with concurrent flood-wind hazards during winter DJF.** The  
 417 F-Score is shown for each CMIP5 AOGCM, MMEM, NCEP, 20CR and Lamb's subjective catalogue  
 418 for the 1980s, 2020s, 2050s and 2080s periods. The LWTs used for calculating the F-Score are  
 419 associated with concurrent multi-basin floods and wind hazards within Great Britain (GB) [24]. The  
 420 1980s MME F-Score were estimated from the mean of n=1,000 boot-strapped samples and all the  
 421 future 2020s, 2050s and 2080s periods are significantly different from these, as the F-Score of the latter  
 422 fall outside the 95% confidence intervals of the 1980s means. The AOGCMs 1980s confidence intervals  
 423 bars are not shown for simplicity because they are vanishingly narrow.  
 424  
 425

426 Summer nocturnal UHI temperatures in tenths of °C for London (UK), were estimated for  
 427 RCP8.5, by using UHI values obtained in a previous study [29] (Figure 6). Our results show that  
 428 AOGCMs replicate nocturnal UHI temperatures, although there is a tendency for underestimation  
 429 by the majority of AOGCMs except HadGEM2-ES and MIROC5 which show good agreement when  
 430 compared to NCEP, 20CR and Lamb's subjective catalogue. We also note that there is less variability  
 431 within the MME than displayed in Figures 3 and 5. Lastly, almost all the AOGCMs and MMEM show  
 432 a statistically significant increase in UHI by the end of 2100, that could translate into an increased  
 433 multi-hazard risk from heatwave and poor air quality events associated with persistent A weather

434 types [29,47,77,78]. The projected increase in the MMEM UHI between the 1980s and 2080s is 0.15 °C  
 435 under RCP8.5. The AOGCMs that show the largest increase in nocturnal UHI temperatures between  
 436 1980s and 2080s are CanESM2, HadGEM2-ES and CCSM4 with respectively 0.23, 0.22 and 0.22 °C.  
 437 Results for RCP4.5 agree with the RCP8.5 projections although the changes are less marked (Figure  
 438 S5). Implied increases in the risk of urban air pollution hazards are potentially conservative given  
 439 policies to phase out conventional cars in the UK by 2050.  
 440  
 441



442  
 443 **Figure 6. As per Figure 5 but for London’s nocturnal UHI in tenths of °C during summer JJA.**  
 444  
 445

446 **4. Discussion and Conclusions**

447 Greater A-type persistence and frequency during summer likely implies more blocking episodes  
 448 with increased risk of poor air quality, drought and heatwaves [1,5,79,80]. A growing number of  
 449 studies propose physical mechanisms that link Arctic Amplification (AA) [81] to more persistent  
 450 weather patterns, which in turn enhance the likelihood of extreme weather events in the northern  
 451 hemisphere mid-latitudes. The AA may affect the polar jet stream by making Rossby waves more  
 452 meridional (or wavier) and by weakening its flow. A wavier and weaker jet stream in summer  
 453 favours more persistent extreme weather and it is also thought to extend ridges northward,  
 454 enhancing such effects [1–3,79,80,82–84]. On the other hand, another study suggests that increasing  
 455 trends in meridional extent of the jet stream, along with blocking events, may be an artefact of the  
 456 methodologies used [85].  
 457

458 Our results support earlier analysis [46], and are consistent with the proposed mechanisms  
 459 linking *observed* AA with mid-latitude weather extremes. On the other hand, AA could have limited  
 460 effect on simulated CMIP5 blocking over Eurasia under RCP8.5 in the second half of the 21<sup>st</sup> century  
 461 [86]. Other work also shows an overall decrease in CMIP5 blocking events over the BI in winter DJF  
 462 and summer JJA, during 2061-2090 (RCP8.5) [62]. Our findings for anticyclonic weather appear to  
 463 contradict this. Although A-type persistence and frequency are equivalent to blocking *per se*, we

464 would expect the studies to agree as both mechanisms involve high pressure weather systems. A  
465 common denominator between our findings and studies of blocking [62,86] is the underestimation of  
466 A-type/blocking events by CMIP5 models. However, further research is needed to reconcile  
467 apparently contradictory findings. Possible explanations are that results depend on the exact spatial  
468 domain and/or suite of AOGCMs analysed in each MME, as well as on the methodology used to  
469 define A-type days and blocking events.

470

471 Less persistent C-types in autumn suggests lower likelihood of heavy rainfall, with reduced  
472 recharge of soil moisture and aquifers at the start of the hydrological year, thereby favouring winter  
473 droughts. Fewer cyclonic days may also translate into less frequent severe gales and flooding  
474 episodes [76], as in GB extreme multi-basin flooding events are strongly associated with C-type  
475 weather over time windows from 1 to 19 days [24]. Conversely, more frequent zonal airflow (W-type)  
476 in winter may counteract some loss of precipitation from the C-type, especially across higher  
477 elevation regions of the north and west BI where there is strong orographic enhancement [87]. Such  
478 changes may also be attributed to AA, however, the physical mechanisms linking AA to changes in  
479 northern hemisphere mid-latitude circulation currently remains an open question.

480

481 From our analyses it is also possible to infer future changes with respect to multi-hazards [15,17],  
482 through the F-Score and nocturnal UHI temperatures. Recent analyses show that in GB nearly  
483 concurrent multi-basin flooding and extreme wind events are driven by selected LWTs mainly  
484 associated with C- and W-types [24]. These multi-hazard events can generate significant economic  
485 losses hence projections of such events may help in evaluating future risks and in improving  
486 resilience. We show that during winter DJF our ensemble of AOGCMs overestimate the F-Score when  
487 compared to NCEP, 20CR reanalyses and Lamb's subjective dataset. Even so, by the end of 2100 the  
488 MMEM shows a statistically significant increase in the F-Score compared with the 1980s within those  
489 same models, suggesting that the risk of concurrent flood-wind impacts may become more severe in  
490 a warmer world.

491

492 Nocturnal UHI temperatures in London modelled by AOGCMs agree with NCEP, 20CR and  
493 Lamb's subjective datasets, although they are slightly underestimated for the 1980s. Nocturnal UHI  
494 severity could increase by 2100 under RCP8.5 (MMEM). Our results confirm an increasing trend of  
495  $\sim 0.3$  °C in nocturnal UHI in London found in an earlier study over the observational period 1950-  
496 2006 [29]. Our findings are also in line with the UK Climate Projections Science Report 2009 [88] which  
497 suggests that intense UHI events are highly correlated with A-type weather patterns, and that in  
498 London, intense UHI summer events could become more severe in the future [89]. However, further  
499 analysis of projections of UHI is needed with a larger AOGCM ensemble to better account for  
500 uncertainty. Our results for UHI also assume an unchanging urban landscape and pattern of artificial  
501 heat sources. Nevertheless, the present findings, when viewed as a significant increase in persistence  
502 and frequency of A-type weather pattern, suggest more favourable conditions for heatwaves and  
503 poor air quality events in London that could negatively impact human health [29,47,77,78,89].

504

505 Finally, we have illustrated how changes in the persistence and frequency of weather patterns  
506 are useful diagnostics of climate model realism and can translate into regional to local weather and

507 climate risks scenarios, which could be helpful for developing narratives for decision-makers.  
508 However, caution needs to be taken when qualitatively converting synoptic weather pattern changes  
509 into local variability because AOGCM skill in reproducing climatic variables at local scales varies  
510 significantly and is not always consistent with observations. This is particularly true for precipitation  
511 where, for example, pressure fields alone are not able to provide reliable local projections [34].  
512

513         With the UK Climate Projections 2018 now partly released and planning underway for the third  
514 UK Climate Change Risk Assessment, weather pattern analysis could help to both evaluate the new  
515 projections and offer ways of explaining changes that are intelligible to a range of user communities.  
516 Similar links to persistence could be made in other regions with established weather pattern  
517 typologies, such as the *Grosswetterlagen* for Europe [90], hydrologically important weather types in  
518 the contiguous United States [91] and Spatial Synoptic Classification for North America [92].  
519  
520



521 **Supplementary Materials:** *Supplementary datasets. Supplementary Data and Methods. Supplementary Figures*, Figure  
522 S1: As per Figure 2 but for RCP4.5, Figure S2: As per Figure 3 but for RCP4.5, Figure S3: As per Figure 4 but for  
523 RCP4.5, Figure S4: As per Figure 5 but for RCP4.5, Figure S5: As per Figure 6 but for RCP4.5. *Supplementary*  
524 *Tables*, Table S1: MME statistical significance of LWTs persistence for RCP8.5, Table S2: The same as Table S1 but  
525 for RCP4.5, Table S3: Sen’s slopes of MMEM seasonal LWTs frequencies for RCP8.5 and RCP4.5.  
526

527 **Author Contributions:** Conceptualization, PDL and RW; methodology, PDL, RW and CF; software, CH and  
528 PDL; formal analysis, PDL; data curation, PDL and CH; writing—original draft preparation, PDL; writing—  
529 review and editing, PDL, RW, JH, CF and GL; supervision, RW, JH and GL.  
530

531 **Funding:** PDL was funded by a Natural Environment Research Council studentship awarded through the  
532 Central England NERC Training Alliance (CENTA <http://www.centa.org.uk/>; Grant No. NE/L002493/1) and by  
533 Loughborough University. CF was supported by the Collaborative Research Centre TRR 181 “Energy Transfer  
534 in Atmosphere and Ocean”, funded by the Deutsche Forschungsgemeinschaft (DFG, German Research  
535 Foundation <https://www.dfg.de/en/>) – Projektnummer 274762653. The APC was funded by CENTA NERC.  
536

537 **Conflicts of Interest:** The authors declare no conflict of interest. The funders had no role in the design of the  
538 study; in the collection, analyses, or interpretation of data; in the writing of the manuscript, or in the decision to  
539 publish the results.

540

541

542

543

544

545

546

547

548

549

550

551

552

553

554

555

556

557

558 **References**

- 559 1. Coumou D, Di Capua G, Vavrus S, Wang L, Wang S. The influence of Arctic amplification  
560 on mid-latitude summer circulation. *Nat Commun* 2018;9:2959. doi:10.1038/s41467-018-  
561 05256-8.
- 562 2. Francis J, Skific N. Evidence linking rapid Arctic warming to mid-latitude weather patterns.  
563 *Philos Trans R Soc London A Math Phys Eng Sci* 2015;373. doi:10.1098/rsta.2014.0170.
- 564 3. Francis JA, Vavrus SJ. Evidence linking Arctic amplification to extreme weather in mid-  
565 latitudes. *Geophys Res Lett* 2012;39. doi:10.1029/2012GL051000.
- 566 4. Francis JA, Vavrus SJ. Evidence for a wavier jet stream in response to rapid Arctic warming.  
567 *Environ Res Lett* 2015;10:14005.
- 568 5. Munich Re. Natural catastrophes 2014: Analyses, assessments, positions. 2015.
- 569 6. Munich Re. NatCatSERVICE - Natural catastrophes in 2018. 2019.
- 570 7. Stott PA, Stone DA, Allen MR. Human contribution to the European heatwave of 2003.  
571 *Nature* 2004;432:610–4. doi:10.1038/nature03089.
- 572 8. Barriopedro D, Fischer EM, Luterbacher J, Trigo RM, García-Herrera R. The Hot Summer of  
573 2010: Redrawing the Temperature Record Map of Europe. *Science* (80- ) 2011;332:220 LP –  
574 224. doi:10.1126/science.1201224.
- 575 9. Bastos A, Gouveia CM, Trigo RM, Running SW. Analysing the spatio-temporal impacts of  
576 the 2003 and 2010 extreme heatwaves on plant productivity in Europe. *Biogeosciences*  
577 2014;11:3421–35. doi:10.5194/bg-11-3421-2014.
- 578 10. Le Tertre A, Lefranc A, Eilstein D, Declercq C, Medina S, Blanchard M, et al. Impact of the  
579 2003 Heatwave on All-Cause Mortality in 9 French Cities. *Epidemiology* 2006;17:75–9.
- 580 11. Sun Y, Zhang X, Zwiers FW, Song L, Wan H, Hu T, et al. Rapid increase in the risk of  
581 extreme summer heat in Eastern China. *Nat Clim Chang* 2014;4:1082.
- 582 12. Muchan K, Lewis M, Hannaford J, Parry S. The winter storms of 2013/2014 in the UK:  
583 hydrological responses and impacts. *Weather* 2015;70:55–61. doi:10.1002/wea.2469.
- 584 13. Kendon M, McCarthy M. The UK's wet and stormy winter of 2013/2014. *Weather*  
585 2015;70:40–7. doi:10.1002/wea.2465.
- 586 14. Matthews T, Murphy C, Wilby RL, Harrigan S. Stormiest winter on record for Ireland and  
587 UK. *Nat Publ Gr* 2014;4:738–40. doi:10.1038/nclimate2336.
- 588 15. Zscheischler J, Westra S, van den Hurk BJJM, Seneviratne SI, Ward PJ, Pitman A, et al.  
589 Future climate risk from compound events. *Nat Clim Chang* 2018;8:469–77.  
590 doi:10.1038/s41558-018-0156-3.

- 591 16. AghaKouchak A, Huning LS, Mazdidasni O, Mallakpour I, Chiang F, Sadegh M, et al. How  
592 do natural hazards cascade to cause disasters? *Nature* 2018;561:458–60. doi:10.1038/d41586-  
593 018-06783-6.
- 594 17. Gill JC, Malamud BD. Reviewing and visualizing the interactions of natural hazards. *Rev*  
595 *Geophys* 2014;52:680–722. doi:10.1002/2013RG000445.
- 596 18. Kappes MS, Keiler M, von Elverfeldt K, Glade T. Challenges of analyzing multi-hazard risk:  
597 a review. *Nat Hazards* 2012;64:1925–58. doi:10.1007/s11069-012-0294-2.
- 598 19. Terzi S, Torresan S, Schneiderbauer S, Critto A, Zebisch M, Marcomini A. Multi-risk  
599 assessment in mountain regions: A review of modelling approaches for climate change  
600 adaptation. *J Environ Manage* 2019;232:759–71.  
601 doi:<https://doi.org/10.1016/j.jenvman.2018.11.100>.
- 602 20. Forzieri G, Feyen L, Russo S, Voutsdoukas M, Alfieri L, Outten S, et al. Multi-hazard  
603 assessment in Europe under climate change. *Clim Change* 2016;137:105–19.  
604 doi:10.1007/s10584-016-1661-x.
- 605 21. Gallina V, Torresan S, Critto A, Sperotto A, Glade T, Marcomini A. A review of multi-risk  
606 methodologies for natural hazards: Consequences and challenges for a climate change  
607 impact assessment. *J Environ Manage* 2016;168:123–32.
- 608 22. UNDRR. Sendai Framework for Disaster Risk Reduction 2015–2030. 2015.
- 609 23. Kargel JS, Leonard GJ, Shugar DH, Haritashya UK, Bevington A, Fielding EJ, et al.  
610 Geomorphic and geologic controls of geohazards induced by Nepal’s 2015 Gorkha  
611 earthquake. *Science* (80- ) 2016;351.
- 612 24. De Luca P, Hillier JK, Wilby RL, Quinn NW, Harrigan S. Extreme multi-basin flooding  
613 linked with extra-tropical cyclones. *Environ Res Lett* 2017;12:114009. doi:10.1088/1748-  
614 9326/aa868e.
- 615 25. Ward PJ, Couasnon A, Eilander D, Haigh ID, Hendry A, Muis S, et al. Dependence between  
616 high sea-level and high river discharge increases flood hazard in global deltas and estuaries.  
617 *Environ Res Lett* 2018;13:84012. doi:10.1088/1748-9326/aad400.
- 618 26. Collet L, Harrigan S, Prudhomme C, Formetta G, Beevers L. Future hot-spots for hydro-  
619 hazards in Great Britain: a probabilistic assessment. *Hydrol Earth Syst Sci* 2018;22:5387–401.  
620 doi:10.5194/hess-22-5387-2018.
- 621 27. De Luca P, Messori G, Wilby RL, Mazzoleni M, Di Baldassarre G. Concurrent wet and dry  
622 hydrological extremes at the global scale. *Earth Syst Dynam Discuss* 2019:1–24.  
623 doi:10.5194/esd-2019-27.
- 624 28. Visser-Quinn A, Beevers L, Collet L, Formetta G, Smith K, Wanders N, et al. Spatio-temporal  
625 analysis of compound hydro-hazard extremes across the UK. *Adv Water Resour*

- 626 2019;130:77–90. doi:<https://doi.org/10.1016/j.advwatres.2019.05.019>.
- 627 29. Wilby RL, Jones PD, Lister DH. Decadal variations in the nocturnal heat island of London.  
628 *Weather* 2011;66:59–64. doi:10.1002/wea.679.
- 629 30. Merz B, Aerts J, Arnbjerg-Nielsen K, Baldi M, Becker A, Bichet A, et al. Floods and climate:  
630 emerging perspectives for flood risk assessment and management. *Nat Hazards Earth Syst*  
631 *Sci* 2014;14:1921–42. doi:10.5194/nhess-14-1921-2014.
- 632 31. Conticello F, Cioffi F, Merz B, Lall U. An event synchronization method to link heavy  
633 rainfall events and large-scale atmospheric circulation features. *Int J Climatol* 2018;38:1421–  
634 37. doi:10.1002/joc.5255.
- 635 32. Farnham DJ, Doss-Gollin J, Lall U. Regional Extreme Precipitation Events: Robust Inference  
636 From Credibly Simulated GCM Variables. *Water Resour Res* 2018;54:3809–24.  
637 doi:10.1002/2017WR021318.
- 638 33. Murawski A, Vorogushyn S, Bürger G, Gerlitz L, Merz B. Do Changing Weather Types  
639 Explain Observed Climatic Trends in the Rhine Basin? An Analysis of Within- and Between-  
640 Type Changes. *J Geophys Res Atmos* 2018;123:1562–84. doi:10.1002/2017JD026654.
- 641 34. Murawski A, Bürger G, Vorogushyn S, Merz B. Can local climate variability be explained by  
642 weather patterns? A multi-station evaluation for the Rhine basin. *Hydrol Earth Syst Sci*  
643 2016;20:4283–306. doi:10.5194/hess-20-4283-2016.
- 644 35. Pattison I, Lane SN. The relationship between Lamb weather types and long-term changes in  
645 flood frequency, River Eden, UK. *Int J Climatol* 2012;32:1971–89. doi:10.1002/joc.2415.
- 646 36. Matthews T, Murphy C, Wilby RL, Harrigan S. A cyclone climatology of the British-Irish  
647 Isles 1871–2012. *Int J Climatol* 2016;36:1299–312. doi:10.1002/joc.4425.
- 648 37. Wilby RL, Wigley TML. Downscaling general circulation model output: a review of methods  
649 and limitations. *Prog Phys Geogr Earth Environ* 1997;21:530–48.  
650 doi:10.1177/030913339702100403.
- 651 38. Xu H, Corte-Real J, Qian B. Developing daily precipitation scenarios for climate change  
652 impact studies in the Guadiana and the Tejo basins. *Hydrol Earth Syst Sci* 2007;11:1161–73.  
653 doi:10.5194/hess-11-1161-2007.
- 654 39. Lamb HH. British Isles Weather types and a register of daily sequence of circulation  
655 patterns, 1861-1971. *Geophysical Memoir* 116, London, HMSO; 1972.
- 656 40. Jones PD, Hulme M, Briffa KR. A comparison of Lamb circulation types with an objective  
657 classification scheme. *Int J Climatol* 1993;13:655–63. doi:10.1002/joc.3370130606.
- 658 41. Jenkinson AF, Collison FP. An Initial Climatology of Gales over the North Sea. *Synoptic*  
659 *Climatology Branch Memorandum No. 62*, Meteorological Office, Bracknell; 1977.

- 660 42. Burt TP, Jones PD, Howden NJK. An analysis of rainfall across the British Isles in the 1870s.  
661 Int J Climatol 2015;35:2934–47. doi:10.1002/joc.4184.
- 662 43. Jones PD, Harpham C, Briffa KR. Lamb weather types derived from reanalysis products. Int  
663 J Climatol 2013;33:1129–39. doi:10.1002/joc.3498.
- 664 44. Tyler JJ, Jones M, Arrowsmith C, Allott T, Leng MJ. Spatial patterns in the oxygen isotope  
665 composition of daily rainfall in the British Isles. Clim Dyn 2016;47:1971–87.  
666 doi:10.1007/s00382-015-2945-y.
- 667 45. Stryhal J, Huth R. Trends in winter circulation over the British Isles and central Europe in  
668 twenty-first century projections by 25 CMIP5 GCMs. Clim Dyn 2018;0:0. doi:10.1007/s00382-  
669 018-4178-3.
- 670 46. Otero N, Sillmann J, Butler T. Assessment of an extended version of the Jenkinson–Collison  
671 classification on CMIP5 models over Europe. Clim Dyn 2018;50:1559–79. doi:10.1007/s00382-  
672 017-3705-y.
- 673 47. Pope RJ, Butt EW, Chipperfield MP, Doherty RM, Fenech S, Schmidt A, et al. The impact of  
674 synoptic weather on UK surface ozone and implications for premature mortality. Environ  
675 Res Lett 2016;11. doi:10.1088/1748-9326/11/12/124004.
- 676 48. Burt TP, Ferranti EJS. Changing patterns of heavy rainfall in upland areas: a case study from  
677 northern England. Int J Climatol 2012;32:518–32. doi:10.1002/joc.2287.
- 678 49. Jones PD, Harpham C, Lister D. Long-term trends in gale days and storminess for the  
679 Falkland Islands. Int J Climatol 2016;36:1413–27. doi:10.1002/joc.4434.
- 680 50. Wetterhall F, Pappenberger F, He Y, Freer J, Cloke HL. Conditioning model output statistics  
681 of regional climate model precipitation on circulation patterns. Nonlinear Process Geophys  
682 2012;19:623–33. doi:10.5194/npg-19-623-2012.
- 683 51. Richardson D, Fowler HJ, Kilsby CG, Neal R. A new precipitation and drought climatology  
684 based on weather patterns. Int J Climatol 2018;38:630–48. doi:10.1002/joc.5199.
- 685 52. Wilby RL, Dalgleish HY, Foster IDL. The impact of weather patterns on historic and  
686 contemporary catchment sediment yields. Earth Surf Process Landforms 1997;22:353–63.
- 687 53. Blenkinsop S, Chan SC, Kendon EJ, Roberts NM, Fowler HJ. Temperature influences on  
688 intense UK hourly precipitation and dependency on large-scale circulation. Environ Res Lett  
689 2015;10:54021. doi:10.1088/1748-9326/10/5/054021.
- 690 54. Fowler HJ, Kilsby CG. A weather-type approach to analysing water resource drought in the  
691 Yorkshire region from 1881 to 1998. J Hydrol 2002;262:177–92.  
692 doi:https://doi.org/10.1016/S0022-1694(02)00034-3.
- 693 55. Wilby RL. The influence of variable weather patterns on river water quantity and quality

- 694 regimes. *Int J Climatol* 1993;13:447–59. doi:10.1002/joc.3370130408.
- 695 56. Tang L, Chen D, Karlsson P, Gu Y, Ou T. Synoptic circulation and its influence on spring  
696 and summer surface ozone concentrations in southern Sweden. *Boreal Environ Res*  
697 2009;14:889–902.
- 698 57. Grundström M, Hak C, Chen D, Hallquist M, Pleijel H. Variation and co-variation of PM10,  
699 particle number concentration, NO<sub>x</sub> and NO<sub>2</sub> in the urban air – Relationships with wind  
700 speed, vertical temperature gradient and weather type. *Atmos Environ* 2015;120:317–27.  
701 doi:<https://doi.org/10.1016/j.atmosenv.2015.08.057>.
- 702 58. Cortesi N, Gonzalez-Hidalgo JC, Trigo RM, Ramos AM. Weather types and spatial  
703 variability of precipitation in the Iberian Peninsula. *Int J Climatol* 2014;34:2661–77.  
704 doi:10.1002/joc.3866.
- 705 59. Domínguez-Castro F, Ramos AM, García-Herrera R, Trigo RM. Iberian extreme precipitation  
706 1855/1856: an analysis from early instrumental observations and documentary sources. *Int J*  
707 *Climatol* 2015;35:142–53. doi:10.1002/joc.3973.
- 708 60. Eiras-Barca J, Lorenzo N, Taboada J, Robles A, Miguez-Macho G. On the relationship  
709 between atmospheric rivers, weather types and floods in Galicia (NW Spain). *Nat Hazards*  
710 *Earth Syst Sci* 2018;18:1633–45. doi:10.5194/nhess-18-1633-2018.
- 711 61. Lorenzo MN, Taboada JJ, Gimeno L. Links between circulation weather types and  
712 teleconnection patterns and their influence on precipitation patterns in Galicia (NW Spain).  
713 *Int J Climatol* 2008;28:1493–505. doi:10.1002/joc.1646.
- 714 62. Woollings T, Barriopedro D, Methven J, Son S-W, Martius O, Harvey B, et al. Blocking and  
715 its Response to Climate Change. *Curr Clim Chang Reports* 2018. doi:10.1007/s40641-018-  
716 0108-z.
- 717 63. Taylor KE, Stouffer RJ, Meehl GA. An Overview of CMIP5 and the Experiment Design. *Bull*  
718 *Am Meteorol Soc* 2011;93:485–98. doi:10.1175/BAMS-D-11-00094.1.
- 719 64. Compo GP, Whitaker JS, Sardeshmukh PD, Matsui N, Allan RJ, Yin X, et al. The Twentieth  
720 Century Reanalysis Project. *Q J R Meteorol Soc* 2011;137:1–28. doi:10.1002/qj.776.
- 721 65. Kalnay E, Kanamitsu M, Kistler R, Collins W, Deaven D, Gandin L, et al. The NCEP/NCAR  
722 40-Year Reanalysis Project. *Bull Am Meteorol Soc* 1996;77:437–71. doi:10.1175/1520-  
723 0477(1996)077<0437:TNYP>2.0.CO;2.
- 724 66. Hulme M, Barrow E. *Climate of the British Isles: present, past and future*. London:  
725 Routledge; 1997.
- 726 67. Lamb HH. Types and spells of weather around the year in the British Isles : Annual trends,  
727 seasonal structure of the year, singularities. *Q J R Meteorol Soc* 1950;76:393–429.  
728 doi:10.1002/qj.49707633005.

- 729 68. Hulme M, Briffa KR, Jones PD, Senior CA, Briffa KR, Jones PD, et al. Validation of GCM  
730 control simulations using indices of daily airflow types over the British Isles. *Clim Dyn*  
731 1993;9:95–105. doi:10.1007/BF00210012.
- 732 69. Jones PD, Osborn TJ, Harpham C, Briffa KR. The development of Lamb weather types: From  
733 subjective analysis of weather charts to objective approaches using reanalyses. *Weather*  
734 2014;69:128–32. doi:10.1002/wea.2255.
- 735 70. Wilby RL. Stochastic weather type simulation for regional climate change impact  
736 assessment. *Water Resour Res* 1994;30:3395–403. doi:10.1029/94WR01840.
- 737 71. Gagniuc PA. *Markov Chains: From Theory to Implementation and Experimentation*. USA,  
738 NJ: John Wiley & Sons; 2017. doi:10.1002/9781119387596.
- 739 72. Spedicato GA. Discrete Time Markov Chains with R. *R J* 2017;9:84–104.
- 740 73. Mann HB, Whitney DR. On a Test of Whether one of Two Random Variables is  
741 Stochastically Larger than the Other. *Ann Math Stat* 1947;18:50–60.  
742 doi:10.1214/aoms/1177730491.
- 743 74. Hamed KH, Ramachandra Rao A. A modified Mann-Kendall trend test for autocorrelated  
744 data. *J Hydrol* 1998;204:182–96. doi:https://doi.org/10.1016/S0022-1694(97)00125-X.
- 745 75. Sen PK. Estimates of the Regression Coefficient Based on Kendall's Tau. *J Am Stat Assoc*  
746 1968;63:1379–89. doi:10.1080/01621459.1968.10480934.
- 747 76. Wilby RL, Quinn NW. Reconstructing multi-decadal variations in fluvial flood risk using  
748 atmospheric circulation patterns. *J Hydrol* 2013;487:109–21. doi:10.1016/j.jhydrol.2013.02.038.
- 749 77. O'Hare GPP, Wilby RL. A Review of Ozone Pollution in the United Kingdom and Ireland  
750 with an Analysis Using Lamb Weather Types. *Geogr J* 1995;161:1–20. doi:10.2307/3059923.
- 751 78. Pope RJ, Savage NH, Chipperfield MP, Arnold SR, Osborn TJ. The influence of synoptic  
752 weather regimes on UK air quality: analysis of satellite column NO<sub>2</sub>. *Atmos Sci Lett*  
753 2014;15:211–7. doi:10.1002/asl2.492.
- 754 79. Tang Q, Zhang X, Francis JA. Extreme summer weather in northern mid-latitudes linked to a  
755 vanishing cryosphere. *Nat Clim Chang* 2013;4:45.
- 756 80. Pfleiderer P, Schleussner C-F, Kornhuber K, Coumou D. Summer weather becomes more  
757 persistent in a 2 °C world. *Nat Clim Chang* 2019. doi:10.1038/s41558-019-0555-0.
- 758 81. Screen JA, Simmonds I. The central role of diminishing sea ice in recent Arctic temperature  
759 amplification. *Nature* 2010;464:1334.
- 760 82. Cohen J, Screen JA, Furtado JC, Barlow M, Whittleston D, Coumou D, et al. Recent Arctic  
761 amplification and extreme mid-latitude weather. *Nat Geosci* 2014;7:627.

- 762 83. Francis JA. Why Are Arctic Linkages to Extreme Weather Still up in the Air? *Bull Am*  
763 *Meteorol Soc* 2017;98:2551–7. doi:10.1175/BAMS-D-17-0006.1.
- 764 84. Francis JA, Vavrus SJ, Cohen J. Amplified Arctic warming and mid-latitude weather: new  
765 perspectives on emerging connections. *Wiley Interdiscip Rev Clim Chang* 2017;8:e474.  
766 doi:10.1002/wcc.474.
- 767 85. Barnes EA. Revisiting the evidence linking Arctic amplification to extreme weather in  
768 midlatitudes. *Geophys Res Lett* 2013;40:4734–9. doi:10.1002/grl.50880.
- 769 86. Woollings T, Harvey B, Masato G. Arctic warming, atmospheric blocking and cold European  
770 winters in CMIP5 models. *Environ Res Lett* 2014;9:14002.
- 771 87. Burt TP, Howden NJK. North Atlantic Oscillation amplifies orographic precipitation and  
772 river flow in upland Britain. *Water Resour Res* 2013;49:3504–15. doi:10.1002/wrcr.20297.
- 773 88. Murphy JM, Sexton DMH, Jenkins GJ, Boorman PM, Booth BBB, Brown CC, et al. UK  
774 Climate Projections Science Report: Climate change projections. Exeter: 2009.
- 775 89. Wilby RL. Constructing Climate Change Scenarios of Urban Heat Island Intensity and Air  
776 Quality. *Environ Plan B Plan Des* 2008;35:902–19. doi:10.1068/b33066t.
- 777 90. Hess P, Brezowsky H. Katalog der Großwetterlagen Europas. Berichte des Deutschen  
778 Wetterdienstes in der US-Zone 33. Deutscher Wetterdienst in d. US-Zone: Bad Kissingen.;  
779 1952.
- 780 91. Prein AF, Bukovsky MS, Mearns LO, Bruyère CL, Done JM. Simulating North American  
781 Weather Types With Regional Climate Models. *Front Environ Sci* 2019;7:36.
- 782 92. Kalkstein LS, Nichols MC, Barthel CD, Greene JS. A new spatial synoptic classification:  
783 application to air-mass analysis. *Int J Climatol* 1996;16:983–1004. doi:10.1002/(SICI)1097-  
784 0088(199609)16:9<983::AID-JOC61>3.0.CO;2-N.
- 785